Evaluation of delamination mechanisms from Charpy impact test in API-X70 steel

Hudison Haskel[1], Ederson Pauletti[1], Juliana P. Martins[2], André L.M.Carvalho[1*]

[1] Department of Materials Engineering, States University of Ponta Grossa-UEPG
[2] Department of Chemical Engineering, Federal Technological University of Paraná-UTFPR
* Corresponding author: andrelmc@uepg.br

Abstract In this article was investigated the mechanisms of delamination phenomena occurs in the X70 steel during fracture process from the Charpy impact testing. Microtexture and Taylor factor map analysis were performed by electron backscatter diffraction (EBSD) technique in two fractured surface regions, namely, in the perpendicular and parallel regions to the propagation fracture direction where delamination occurred. As result, was observed two types of delaminations during fracture process, the crack arrester-type delamination and crack divider-type delamination. The main microtexture components obtained in the perpendicular and parallel regions to the direction of fracture propagation from orientation distribution function (ODF) were (221) [1-10] (223) [1-10] (112) [1-3 -2] (332) [023] and (223) [0-32] and (332) [1-10] orientations, respectively. It was also observed the presence of the (100) planes and Taylor factor value close to 2.7 in the respective regions investigated, consequently, a smaller stored energy was observed.

Keywords Delamination, Charpy impact test, crystallography orientation

1. Introduction

The transport of oil and gas through pipelines requires steels that are characterized by a combination of high strength and toughness, these steels are specified by the API 5L standard. However, during the fracture process by Charpy impact test, these steels exhibit the phenomenon known as delamination. This delamination can be attributed to crystallographic texture, intergranular fracture along grain boundaries of retained austenite, segregation of elements such as phosphorus and sulfur, microstructural anisotropy, banding, inclusions and aligned particles [1]. In this context many studies have been conducted to determine the relationship between microstructure and mechanical properties, where the technique by electron backscatter diffraction (EBSD) has been gained the ability to relate the spatial distribution of plastic deformation with the microstructural characteristics. Besides it allows a better understanding of the mechanisms responsible for the nucleation and propagation of cracks from delamination, which is a major problem in HSLA steels [2,3].The aim of present work is to investigate the mechanisms of delamination phenomena takes place in the API 5L X70 steel during fracture process from the Charpy impact testing in specimens with L-T and T-L orientations. Evaluation of microtexture and Taylor factor mapping were performed from the EBSD technique in two regions, namely, in the perpendicular and parallel regions to the propagation fracture direction where delamination occurred.

2. Experimental procedures

2.1 Material

The material used in this investigation was microalloyed steel specified by API 5L Grade X70 standards. The same was obtained by thermomechanical treatment by controlled rolling. The chemical composition obtained by optical spectrometry technique is shown in Table 1:

Table 1. Chemical composition of API X 70 steel

C	Si	Mn	P	Al	Cu	S
0.14	0.27	1.45	0.01	0.05	0.03	0.00076
Nb	V	Ti	Cr	Ni	Mo	
0.051	0.041	0.018	0.0005	0.001	0.0045	

2.2 Procedures

2.2.1 Charpy impact testing

Charpy impact testing specimens were removed from the orientation and dimensions according to ASTM E-23 [4], as can be seen in Fig. 1.

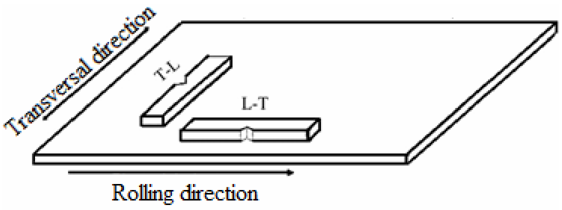

Figure 1. Schematic drawing of the orientation notch specimens

The tests were carried out in a range of temperature variation at 27°C up to -196°C, the specimens were immersed in a cryogenic bath of nitrogen and anhydrous alcohol liquids for 10 minutes, after that the same were withdrawn of the mixture and positioned on the machine. To increase the accuracy of this procedure the hammer would only be released whether all process occurred within 8 seconds.

2.2.2 Microtexture

Microtexture analyses were performed by EBSD technique. To carry out these measurements were used two samples from the fractured specimens in the L-T orientation by impact testing at -25 °C and 226J of absorbed energy in the ductile brittle transition temperature region. The surface specimens analyzed were carried out in the perpendicular region to the direction of fracture propagation and near the edges of the crack generated by crack divider-type delamination, as shown in Fig. 2a), another analysis was performed parallel to the direction of fracture propagation and near the edge separation caused by delamination, as shown in Fig. 2b). Samples were polished in the solution of OP-S (colloidal silica), and then etched with Nital 2%. For EBSD data collection was used software TSL 5 IOM Data collection and for data processing was used software OIM Analysis 5. The scanning electron microscope used for performing of such measures was the EDAX TSL EVO MA 10.

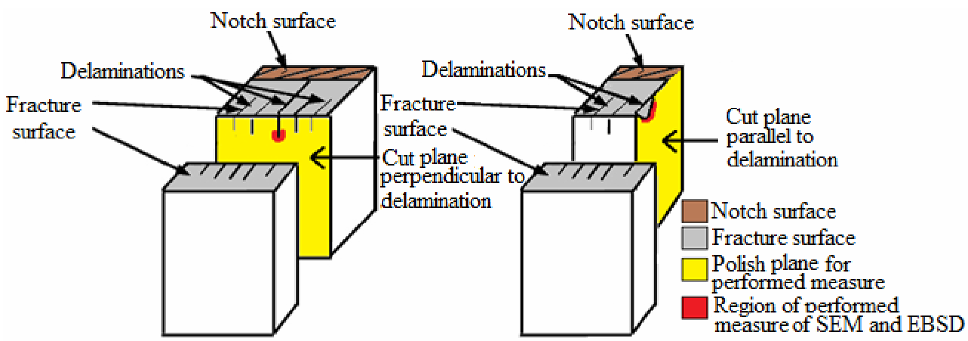

Figure 2. Schematic representation of removed samples for performing EBSD. a) Cut plane of the perpendicular direction of fracture propagation, b) Cut plane in the parallel region to the direction of fracture propagation.

3. Results and Discussion

3.2 Charpy impact testing

Fig. 3a) shows the curve of absorbed energy versus temperature for L-T and T-L orientations. It is possible to notice that there was a greater dispersion of energy values for the samples of L-T orientation when compared to the T-L orientation. At the lower upper shelf energy where the cleavage fracture occurs, both directions have obtained the same amount of energy, 5J. The L-T orientation has a higher upper shelf energy regarding T-L orientation, consequently this direction has higher absorbed energy for all temperatures. Concerning the ductile-brittle transition temperature, the L-T orientation has also obtained the highest absorbed energy values as a function of orientation, as can be seen in Fig. 3b).

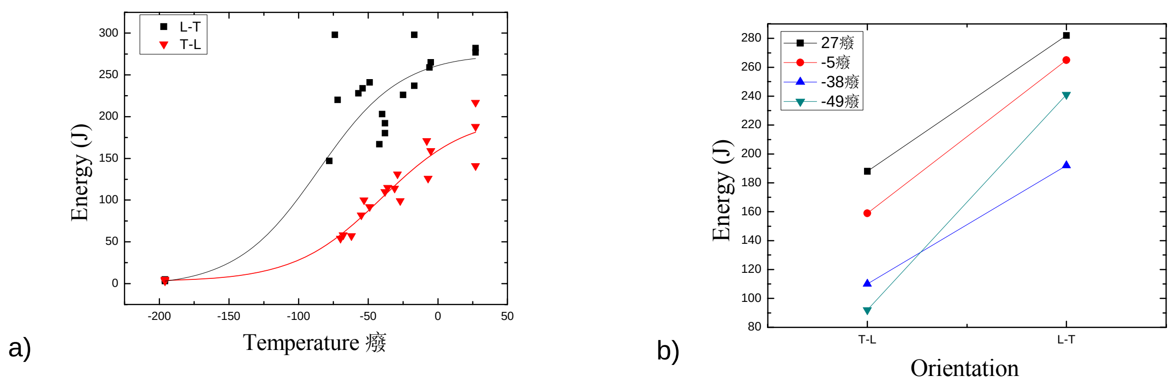

Figure 3. Charpy impact testing a) as a function of temperature, b) as a function of the orientation (for some temperatures)

The ductile-brittle transition temperature was estimated by comparing the percentage of ductile fracture area following the specifications of ASTM E-23[4]. Specimens with L-T orientation showed range lower values of transitions temperature between -38°C to -57°C, while the specimens with T-L orientation exhibited a greater range of the transition temperature values between -8 ° C up to -38 ° C.

3.3. Aspects of delamination phenomenon

Fig. 5) shows fractured surface samples with delaminations from the Charpy impact test. In Fig. 5a) is possible to observe crack arrester-type delamination from the specimen tested at -5°C and 265J of absorbed energy. Fig. 5b) also shows a set of crack divider- type delamination from the specimen tested at -36°C and 100J of absorbed energy.

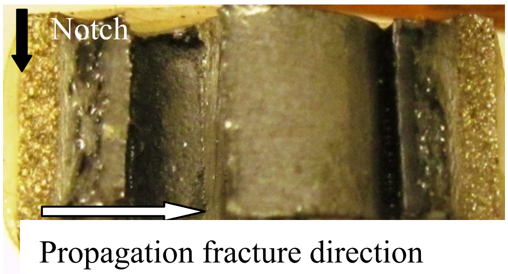

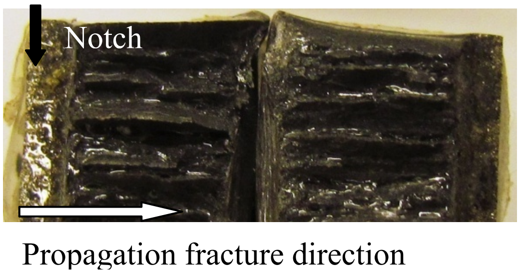

a) b)

Figure 4. Fractured surface by impact test showing the phenomenon of delamination. a) Crack arrester-type delamination, b) Crack divider-type delamination

It can be seen in Fig. 4a) the crack arrester-type delamination is formed perpendicular to the propagation fracture direction and parallel to the notch, while the crack divider-type delamination (Fig. 4b)) occurs parallel to the propagation fracture direction and perpendicular at notch. Cracks arrester-type delaminations are known by their beneficial effect to increase upper shelf energy [5], this suggests a higher tendency of the L-T orientation specimens present crack arrester-type delamination, which may contribute to increase of energy values for L-T orientation independent on the temperature used, as can be seen in Fig 3a).

3.4. Microtexture

Fig. 5 shows an image obtained by scanning electron microscopy in the regions in front of propagated crack by crack divider-type delamination, the distribution map of orientations, the inverse pole figure, the orientation distribution function (ODF) for Bunge angle Φ_2 = 45°, and the pole figures of the (100) and (110) planes. Quantification of microtexture was made by EBSD technique, with the following parameters: Fig. 5b) was used step size of 1 micron and 1000 X magnification and Fig. 5c) was used step size of 3 microns and a magnification of 3000X.
From Fig. 5b) is possible to notice the presence of dark regions, where shows a crack produced by the formation of delamination. The remaining points may be regions of perlite, which have very

thin lamella (about 200nm). As the distance between layers is smaller than the step size used, the occurrence to indexation of crystallographic planes to these regions was not possible, resulting in dark regions. Another plausible explanation is associated to the material deformation, which can contribute to the accumulation of dislocations at grain boundaries, resulting in the non-indexed regions. In Fig. 5b) there is a grain size distributions quite heterogeneous and the absence of (100) plans. While in Fig.5c) shows the propagated crack region by delamination, the same propagates in the grain boundary, featuring an intergranular fracture mechanism. It is confirmed by separation of grains with [111]||ND and [101]||ND texture components indicated by 1 up to 5 grains, respectively.

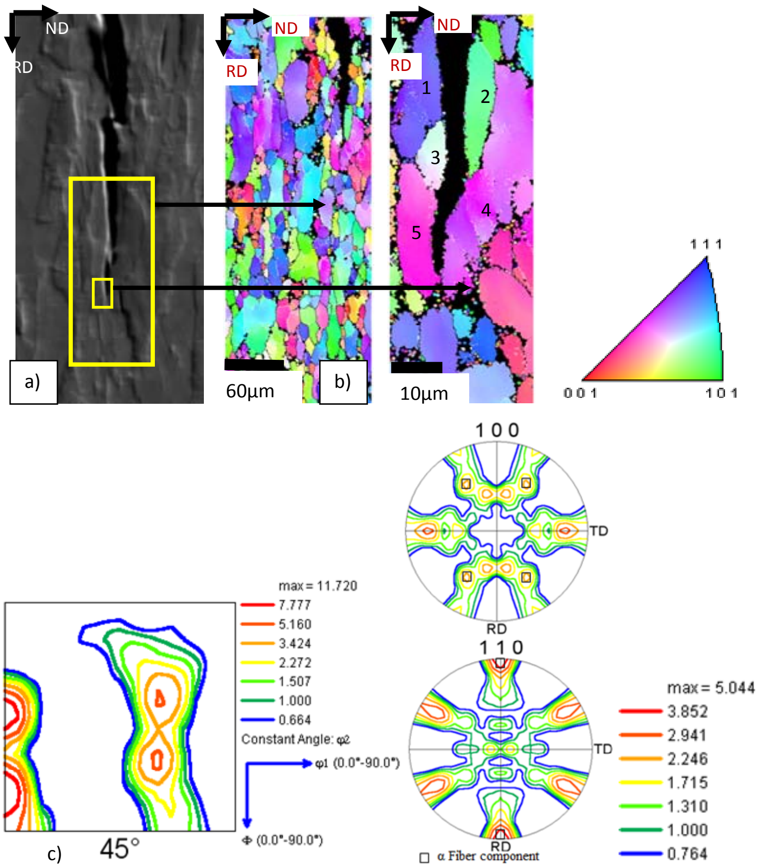

Figure 5. Microtexture in the region near the crack delaminated. a) SEM from the scanned region, b) distribution maps of orientation and inverse pole figure c) orientation distribution function (ODF) and pole figures.

It is well known that intergranular propagation occurs through high angle boundaries. In this context the Fig. 6 shows the misorientation obtained by EBSD technique from the scanned region (Fig 5b)). For generation of statistical data points only disorientation greater than 2° was considered. It is possible to see at Fig. 6 that approximately 42% of the misorientation angles between adjacent grains are smaller than 10° (low angle boundaries) while the other 58% are distributed randomly between 10° and 110°, indicating a high grain boundary angle.

For the generation of pole figures and ODF shown in Fig 5c) was used an orientation map from Fig. 5 b) which provides a better precision in the information due to its higher scanned area. The ODF shown in Fig. 5c) reveals that the orientations have α fiber components. The main components obtained from ODF are (221) [1-10] (223) [1-10] (112) [1-3 -2] and (332) [023] orientations. Pole figures shown in Fig. 5c) confirm the presence of the α fiber components identified by the ODF.

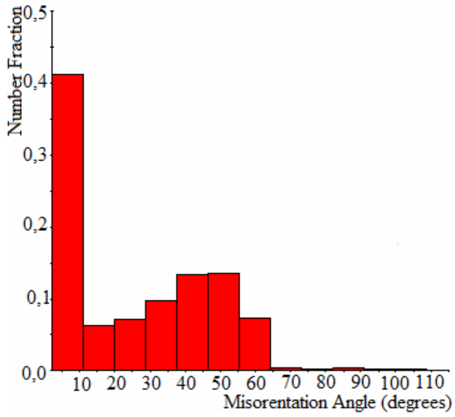

Figure 6. Misorientation angles between adjacent grains near to edges of delamination

Furthermore, materials with crystallographic plane with (100) orientation aligned in the rolling direction show a strong tendency to occur cleavage fracture during impact [1,2,6,7,8,9,10]. To identify whether in this case occurred the separation of the (100) planes were measured microtexture on the edge of the fractured surface where was generated the delamination. This sample was the same used in the analysis of Fig. 6b), but using step size of 1 micron and 1000X magnification, and the results obtained are displayed in Fig. 7. It can be observed in Fig. 7a) the difference of depth between the ferrite and pearlite. While in Fig. 7b) shows the distribution orientations map, there is a heterogeneous distribution of grain sizes and a few areas where there were not indexing of the plans, there is also the presence of (100) plans. The ODF to Bunge angle $\Phi_2 = 45°$ is shown in Fig 7c) and its indexing shows the main texture components was (223) [0-32] and (332) [1-10]. The pole figures are shown in Fig. 7d) where it is possible to notice that higher centering occurred in the (111) plane, however, it also notice that occurred to the (100) plane and indexing of some components reveals the presence of {100} planes families and the <011> families directions. As seen in Fig.5c) the crack nucleated by delamination separated grains with (111)||ND and (101)||ND texture components. It is evident that in this case should be noticed, the presence of the (111)||ND components close to the delamination, confirming the separation of ferrite plans. However the presence of the (100) planes was also confirmed. Whereas when if analyzes the microtexture, it cannot confirm whether this is a general rule for the nucleation of delamination in the material under study.

Experimentally, it is known that the stored energy during deformation changes with the crystallographic orientation of the grains. The Taylor factor is a parameter that correlates to macroscopic deformation behavior with microstructural characteristics of the material [11]. According to the theory of plasticity, the stored energy increases with the Taylor factor which in turn, depends on the crystallographic orientation of the grain in relation to the direction of applied stress [12]. The Taylor factor is defined as:

$$M = \sum \delta\gamma_i / \delta\varepsilon \tag{1}$$

Where $\delta\gamma_i$ represent shear portions in each of activated sliding systems in determinate grain while the sample receives a macroscopic deformation $\delta\varepsilon$ [13].

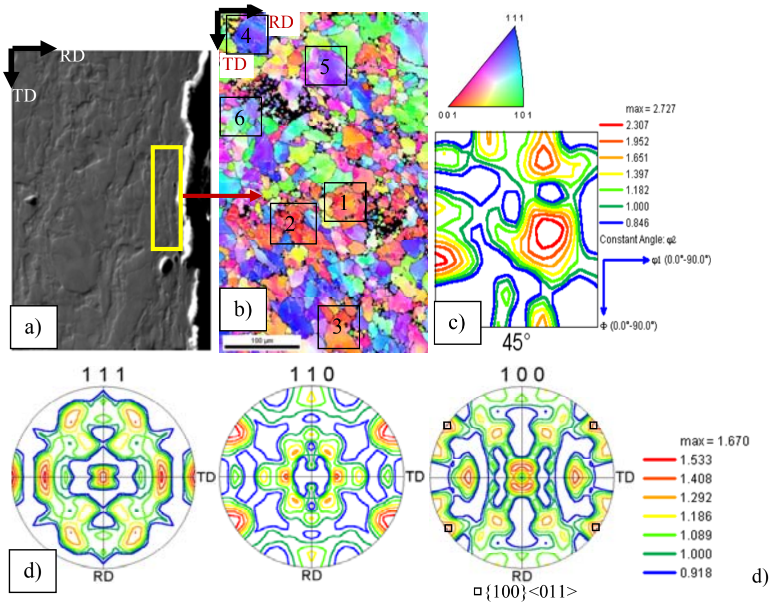

Figure 7. Microtexture analysis by EBSD. a) SEM scanning region, b) Distribution maps of orientation, magnification of 1000X, c) Inverse pole figure and ODF, d) pole figures

Fig. 8 shows the mapping of Taylor factor in front of the crack region for sample shown in Fig. 5b). It is possible to note in Fig. 8a) that mapping shows the separating generated by propagation crack occurs with grains with different Taylor factor values, indicating that the crack delamination intergranular propagate mode. The first and second grains were separated with factor Taylor value around 4.8 and 3.5, respectively. The same situation took place for 5 and 7 grains. Already the 3 and 4 grains also show Taylor factor values in the range of 3.0 and 3.6 respectively, the same has occurred with 5 and 6 grains. It notes that approximately 14% of the grains have Taylor factor values between 4.7 and 4.8 and close to 57% of the grains have Taylor factor values between 2.9 and 3.6.

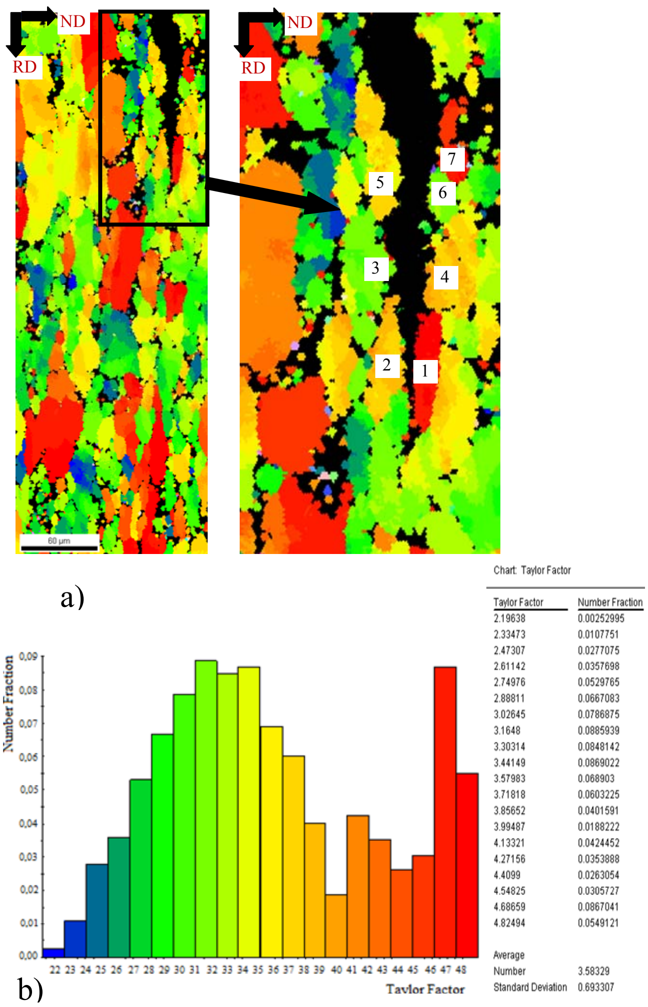

Taylor Factor	Number Fraction
2.19638	0.00252995
2.33473	0.0107751
2.47307	0.0277075
2.61142	0.0357698
2.74976	0.0529765
2.88811	0.0667083
3.02645	0.0786875
3.1648	0.0885939
3.30314	0.0848142
3.44149	0.0869022
3.57983	0.068903
3.71818	0.0603225
3.85652	0.0401591
3.99487	0.0188222
4.13321	0.0424452
4.27156	0.0353888
4.4099	0.0263054
4.54825	0.0305727
4.68659	0.0867041
4.82494	0.0549121
Average	
Number	3.58329
Standard Deviation	0.693307

Figure 8. Mapping of Taylor Factor. a) Scanned region, b) Histogram of number fractions

Besides, in the Fig. 9 shows the mapping of Taylor factor from the sample region shown in Fig. 7b). In the Fig. 9 is possible to observe that approximately 55.34% of the grains have Taylor factor between 2.7 and 3.4.

The stored energy in low carbon steels can be different conform to the sequence: $E_{(110)} > E_{(111)} > E_{(211)} > E_{(100)}$ where hkl plans are related to rolling plans in each grain (12). Thus a comparison can be made from the 1, 2 and 3 numbered regions of the following Figs. 7b) and 9a), where is observed the presence of the (100) planes and Taylor factor value close to 2.7 in the respective regions, consequently, a smaller stored energy was absorbed. Whereas, the 4, 5 and 6 numbered regions of the same figures show a predominance of the (111) planes and Taylor factor value close to 4.5, but the number fraction of grains with this Taylor factor value is low (about 1.53).

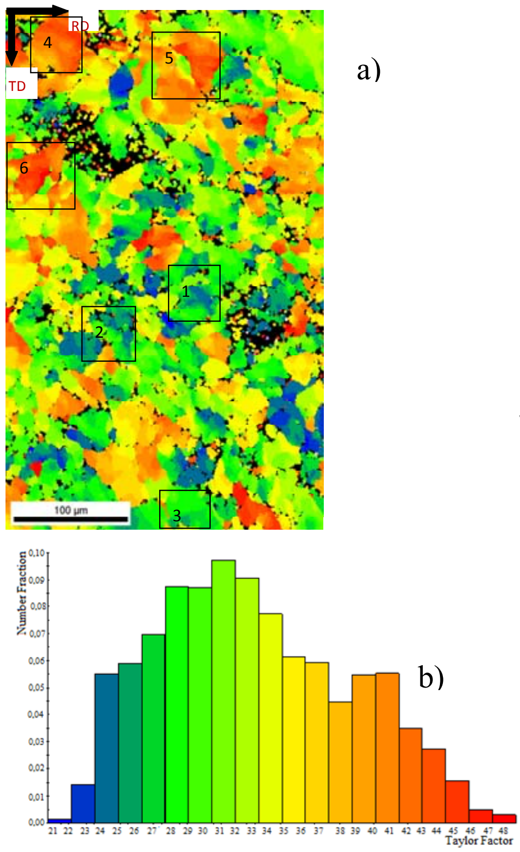

Chart: Taylor Factor

Taylor Factor	Number Fraction
2.14486	0.00141613
2.28297	0.0141161
2.42109	0.0551689
2.55921	0.0589427
2.69732	0.0697822
2.83544	0.0872654
2.97356	0.087077
3.11167	0.0973666
3.24979	0.0906098
3.38791	0.0772244
3.52602	0.0614059
3.66414	0.0594248
3.80226	0.0448417
3.94038	0.0549128
4.07849	0.055312
4.21661	0.0348082
4.35472	0.0271551
4.49284	0.0153816
4.63096	0.0048962
4.76907	0.00289252
Average	
Number	3.29088
Standard Deviation	0.567508

Figure 9. Mapping of Taylor Factor a) Scanned region, b) Histogram of number fractions

4. Conclusions

Charpy impact testing showed that specimens with L-T orientation absorbed more energy than specimens with T-L orientation. It was observed two types of delaminations during fracture process, the crack arrester-type delamination and crack divider-type delamination. The first type propagates parallel to the notch, while the second propagates perpendicular to notch. Crack arrester-type delamination tends to increase upper shelf energy during Charpy impact testing, and both types of delaminations tend to disappear with decreasing temperature.

The results obtained by EBSD technique shows the propagation mode of a crack generated by a divider-type delamination was intergranular. The main microtexture components obtained in the perpendicular region to the direction of fracture propagation from ODF were (221) [1-10] (223) [1-10] (112) [1-3 -2] and (332) [023] orientations. While in the parallel region to the direction of fracture propagation the (223) [0-32] and (332) [1-10] orientations were the main microtexture components.

The Taylor factor analysis display the difference in the Taylor factor values with crystallographic orientation, as expected. It was also observed the presence of the (100) planes and Taylor factor value close to 2.7 in the respective regions investigated, consequently, a smaller stored energy was observed. This confirms the fracture mechanisms from the delaminations are given by little plastic deformation, namely, brittle fracture.

Acknowledgements

The authors thank the USIMINAS by providing the material under study, the UFF-Federal Fluminense University by performing the EBSD measurements. The CAPES by providing scholarship and financial support from the project (PNPD- Case N°. 23038.008242/2010-08)

References

[1] M.S. Joo, D.W. Suh, J.H Bae, H.K.D.H. Bhadeshia, Role of delamination and crystallography on anisotropy of Charpy toughness in API-X80 steel. Materials Science and Engineering A, 546, (2012) 314-322.

[2] H. Yu, Influences of microstructure and texture on crack propagation path of X70 acicular ferrite pipeline steel. Journal of University of Science and Technology Beijing, 15, (2008) 683-687.

[3] P. Shanmugam, S.D Pathak, Some studies on the impact behavior of banded microalloyed steel. Engineering fracture mechanics, 53, (1996) 991-1005.

[4] AMERICAN SOCIETY FOR TESTING AND MATERIALS. Standard Test Methods for Notched Bar Impact Testing of Metallic Materials: ASTM E23. New York: ASTM International, 2002.

[5] M. Jafari, J. Kimura, K. Y. Tsuzakik. Enhancement of upper shelf energy through delamination fracture in 0,05 pct P doped High Strength steel. Metallurgical and materials transactions A, 43A (2012), 2453-2465.

[6] T. Inoue, F.Yin, J. Kimura, Y. Tsuzakik, S. Ochiai, Delamination effect on impact properties of ultrafine-grained low carbon steel processed by warm caliber rolling. Metallurgical and materials transactions A, 41, (2009) 341-355.

[7] C. J. Baczynski, J. J. Jonas, L. E. Collins, The influence of rolling practice on notch toughness and texture development in high-strength linepipe. Metallurgical and materials transactions A, 30, (1999) 3045-3054.

[8] J. I. Verdeja, J. Asensio, J. A. Pero-Sanz, Texture, formability, lamellar tearing and HIC susceptibility of ferritic and low carbon steels. Materials characterization, 50, (2003) 81-86.

[9] W. Yan, W. Sha, L. Zhu, W. Wang, Y. Shan, K. Yang, Delamination Fracture Related to Tempering in a High-Strength Low-Alloy Steel. Metallurgical and materials transactions A, 41 A, (2010) 149-161.

[10] H. Jian, F. Jiang, L. Wei, X. Zheng, K. Wen, Crystallographic mechanism for crack propagation in the T7451 Al-Zn-Mg-Cu alloy. Materials Science and Engineering A, 527, (2010) 5879-5882.

[11] F. Yin, T. Hanamura, T, Inque, K. Nagai, Fiber texture and substrutural features in the caliber-rolled low-carbon steels. Metallurgical and materials transactions A, 35 A, (2004) 665-677.

[12] S.F. Castro, J. Gallego, F. J. F. Landgraf, H. J. Kestenbach, Estudo da laminação de encruamento em aços elétricos semi-processados: correlação como os fatores de Taylor. 60° Congresso Anual da ABM, 60°, (2005) 9.

[13] C.S.C. Viana, A. S. Paula, Texturas de deformação. II workshop sobre Textura e Relações de Orientação: deformação plástica, recristalização e crescimento de grão, 2, (2003) 35-54.